

Discrete effects on some boundary schemes of multiple-relaxation-time lattice Boltzmann model for convection-diffusion equations

Yao Wu^{a,b}, Yong Zhao^{a,b}, Zhenhua Chai^{a,b}, Baochang Shi^{a,b,*}

^a*School of Mathematics and Statistics, Huazhong University of Science and Technology, Wuhan 430074, China*

^b*Hubei Key Laboratory of Engineering Modeling and Scientific Computing, Huazhong University of Science and Technology, Wuhan 430074, China*

Abstract

In this paper, we perform a more general analysis on the discrete effects of some boundary schemes of the popular one- to three-dimensional $DnQq$ multiple-relaxation-time lattice Boltzmann model for convection-diffusion equation (CDE). Investigated boundary schemes include anti-bounce-back(ABB) boundary scheme, bounce-back(BB) boundary scheme and non-equilibrium extrapolation(NEE) boundary scheme. In the analysis, we adopt a transform matrix \mathbf{M} constructed by natural moments in the evolution equation, and the result of ABB boundary scheme is consistent with the existing work of orthogonal matrix \mathbf{M} . We also find that the discrete effect does not rely on the choice of transform matrix, and obtain a relation to determine some of the relaxation-time parameters which can be used to eliminate the numerical slip completely under some assumptions. In this relation, the weight coefficient is considered as an adjustable parameter which makes the parameter adjustment more flexible. The relaxation factors associated with second moments can be used to eliminate the numerical slip of ABB boundary scheme and BB boundary scheme while the numerical slip can not be eliminated of NEE boundary scheme. Furthermore, we extend the relations to complex-valued CDE, several numerical examples are used to test the relations.

Keywords: multiple-relaxation-time Lattice Boltzmann method, discrete effect, convection-diffusion equations, boundary scheme

1. introduction

In recent years, the lattice Boltzmann method (LBM) has gained much attention, and has been widely used in many fields [1, 2, 3, 4]. The LBM has some distinct advantages over traditional methods in dealing with Navier-Stokes equations [5, 6, 7, 8, 9] and convection-diffusion equations (CDEs) [10, 11, 12, 13, 14, 15]. One of the advantages of LBM is dealing with the complex boundary conditions in porous media [16, 17, 18, 19, 20, 21]. When

*Corresponding author

Email address: shibc@hust.edu.cn (Baochang Shi)

we solve the macroscopic partial differential equation, there are always discrete errors in the numerical scheme, the boundary discrete effect exists between the real boundary condition and the numerical solution in the boundary point.

To our knowledge, the discrete effect of the bounce-back(BB) scheme was first discussed for the Poiseuille flow. Ginzburg and Adler [22] first performed a boundary condition analysis for the face-centered-hypercubic lattice Boltzmann (LB) model applied to the Poiseuille flow and a plane stagnation flow. After that, He *et al.* [23] analyzed the discrete effect of BB boundary scheme in the Bhatnagar-Gross-Krook (BGK) model, and found that the relaxation time τ has a significant influence on the BB scheme for the no-slip boundary condition. In a similar way, Guo *et al.* [24] studied the existing discrete effect of the discrete Maxwell's diffuse-reflection (DMDR) scheme and the combined bounce-back/specular-reflection (CBBSR) scheme. Then, they simulated the Poiseuille flow in the slip flow regime with the multiple-relaxation-time (MRT) LB model, and found that the BGK model cannot yield correct results in this regime owing to the discrete effect [25]. Due to find that the boundary schemes considered in Refs. [24, 25] are non-local, they are not suitable for fluid flows in complex geometries, Chai *et al.* [26] developed a local scheme combined halfway bounce-back boundary condition and full diffusive boundary condition for microscale gas flows in complex geometries, and illustrated that to realize the exact slip boundary condition, the discrete effect must be included and corrected. Lu *et al.* [27] proposed an immerse boundary MRT LB model, and presented a special relaxation between two relaxation time parameters in which can reduce the numerical boundary slip effectively. Recently, Ren *et al.* [28] analyzed the discrete effects in the DMDR and CBBSR schemes for the rectangular LBE, and presented a reasonable approach to overcome these discrete effects in these two schemes.

We noted that all of above works focus on the discrete effect of BB boundary scheme for fluid flows. Subsequently, there are also some works on the discrete effect of anti-bounce-back (ABB) boundary schemes for CDEs. Zhang *et al.* [29] presented a general ABB boundary scheme of the BGK model for CDEs. They performed an analysis on the discrete effect of the ABB boundary condition, and suggested that there is a numerical slip related to the lattice size in the diffusion of Couette flow between solid walls, which cannot be eliminated in the BGK model. Then, Cui *et al.* [30] analyzed the ABB boundary condition of the MRT model for CDEs. They presented a theoretical analysis on the discrete effect of the ABB boundary scheme for the simple problems with a parabolic distribution in one direction, and observed that the numerical slip can be eliminated in the MRT LB model by choosing the free relaxation parameters properly. However, the analysis is limited to some special MRT LB models, e.g., D2Q4, D2Q5, and D2Q9 model. Recently, based on the two-relaxation-times(TRT) model, Ginzburg *et al.* [31] presented a more general relation between the two relaxation factors through equating the set of closure relations of the given boundary scheme to the Taylor expansion. In this work, based on the existing works [30], we firstly conduct the discrete effect on the ABB boundary scheme of the more general MRT model composed of the natural moments for CDEs, and then derived a relation with four parameters : the weight coefficient, the relaxation factors s_1 and s_2 associated with first

and second moments and a model parameter θ for adjustment to eliminate the numerical slip. After that, we conduct the discrete effect on BB boundary condition and non-equilibrium extrapolation (NEE) boundary condition, observed that the discrete effect can be eliminated when $s_1 + s_2 = 2$ on BB boundary condition and can not be eliminated on NEE boundary condition. Furthermore, we observed that the relations is applicable to both real- and complex-valued problems, and has a general expression from one to three dimensions.

The paper is organized as follows. In Sec. II, we introduce the MRT model composed of natural moments. Then we derive the equivalent finite-difference scheme of the MRT model for CDEs, and discuss the discrete effects on the ABB, BB, NEE boundary conditions in Sec. III. Numerical tests are performed in Sec. IV. Finally, we give a brief summary in Sec. V.

2. MRT LB model for convection-diffusion equation

Firstly, we introduce the MRT model composed of the natural moments for CDEs. The n -dimensional (nD) CDEs can be written as

$$\partial_t \phi + \nabla \cdot (\phi \mathbf{u}) = \nabla \cdot (D \nabla \phi) + R, \quad (1)$$

where ϕ is a scalar function of position \mathbf{x} and time t , ∇ is the gradient operator with respect to the position \mathbf{x} in n dimensions. D is the diffusion coefficient, \mathbf{u} is the convection velocity and R is the source term.

The evolution equation of the MRT model with $DnQq$ lattice for the CDE can be written as

$$\text{Collision} : f_i(\mathbf{x}, t)^+ = f_i(\mathbf{x}, t) - (\mathbf{M}^{-1} \mathbf{S} \mathbf{M})_{ik} (f_k(\mathbf{x}, t) - f_k^{eq}(\mathbf{x}, t)) + \delta_t [\mathbf{M}^{-1} (\mathbf{I} - \frac{\theta \mathbf{S}}{2}) \mathbf{M}]_{ik} R_k, \quad (2)$$

$$\text{Streaming} : f_i(\mathbf{x} + \mathbf{c}_i \delta_t, t + \delta_t) = f_i(\mathbf{x}, t)^+$$

where δ_t is time step, \mathbf{I} is the identity matrix, and \mathbf{S} is a diagonal relaxation matrix with non-negative elements. The transformation matrix \mathbf{M} is composed of natural moments [32]. θ is a real parameter, corresponding to the MRT model [30] for $\theta = 1$ and a scheme in Ref. [33] for $\theta = 0$, respectively. $f_i(\mathbf{x}, t)$ and $f_i^{eq}(\mathbf{x}, t)$ are the distribution function and equilibrium distribution function (EDF) associated with the discrete velocity \mathbf{c}_i at position \mathbf{x} and time t respectively, and $f_i(\mathbf{x}, t)^+$ is the distribution function after collision. And to simplify the derivation, only the following linear EDF is considered here,

$$f_i^{eq}(\mathbf{x}, t) = \omega_i \phi (1 + \frac{\mathbf{c}_i \cdot \mathbf{u}}{c_s^2}), \quad (3)$$

where ω_i is the weight coefficient, c_s is the so-called lattice sound speed. R_i is the discrete source term, and can be defined as

$$R_i = \omega_i R. \quad (4)$$

Firstly, for the D1Q3 model, the set of discrete velocities are $\mathbf{c} = \{-1, 0, 1\}c$, where $c = \delta_x/\delta_t$ with δ_x being the lattice spacing. The transformation matrix $\mathbf{M} = (\mathbf{c}_{ix}^m)(m = 0, 1, 2)$, which can be expressed as $\mathbf{M} = \mathbf{C}_d\mathbf{M}_0$ [34],

$$\mathbf{M}_0 = \begin{pmatrix} 1 & 1 & 1 \\ -1 & 0 & 1 \\ 1 & 0 & 1 \end{pmatrix}. \quad (5)$$

$$\mathbf{C}_d = \text{diag}(1, c, c^2), \quad (6)$$

$$\mathbf{S} = \text{diag}(s_0, s_1, s_2). \quad (7)$$

As for the D2Q9 model, the discrete velocities can be given by

$$\mathbf{c} = \begin{pmatrix} 0 & 1 & 0 & -1 & 0 & 1 & -1 & -1 & 1 \\ 0 & 0 & 1 & 0 & -1 & 1 & 1 & -1 & -1 \end{pmatrix} c, \quad (8)$$

and the transformation matrix as $\mathbf{M} = (\mathbf{c}_{ix}^m \mathbf{c}_{iy}^n) = \mathbf{C}_d\mathbf{M}_0$, ($m, n = 0, 1, 2, m + n \leq 2$),

$$\mathbf{M}_0 = \begin{pmatrix} 1 & 1 & 1 & 1 & 1 & 1 & 1 & 1 & 1 \\ 0 & 1 & 0 & -1 & 0 & 1 & -1 & -1 & 1 \\ 0 & 0 & 1 & 0 & -1 & 1 & 1 & -1 & -1 \\ 0 & 1 & 0 & 1 & 0 & 1 & 1 & 1 & 1 \\ 0 & 0 & 1 & 0 & 1 & 1 & 1 & 1 & 1 \\ 0 & 0 & 0 & 0 & 0 & 1 & -1 & 1 & -1 \\ 0 & 0 & 0 & 0 & 0 & 1 & 1 & -1 & -1 \\ 0 & 0 & 0 & 0 & 0 & 1 & -1 & -1 & 1 \\ 0 & 0 & 0 & 0 & 0 & 1 & 1 & 1 & 1 \end{pmatrix}. \quad (9)$$

$$\mathbf{C}_d = \text{diag}(1, c, c, c^2, c^2, c^2, c^3, c^3, c^4), \quad (10)$$

$$\mathbf{S} = \text{diag}(s_0, s_1, s_1, s_2, s_2, s_2, s_3, s_3, s_4). \quad (11)$$

In the present MRT model, the macroscopic variable ϕ should be computed by

$$\phi = \sum_i f_i + \frac{\theta R}{2} \delta t. \quad (12)$$

50 3. Discrete effects of some boundary schemes

We now analyze the discrete effects of these boundary scheme in the framework of the MRT model for CDE. For simplicity, we conducted an analysis of Dirichlet boundary conditions for the simple steady problems with a parabolic distribution in one direction.

3.1. Equivalent difference equation of the MRT model

Firstly, we consider the D1Q3 MRT model for one-dimensional steady problems with const R , and set the distribution function as $f_i^j = f_i(x_j)$, with x_j being a discrete grid point. To make the derivation easier to understand, we rewrite Eq. (2) as

$$f_i^j = \begin{cases} f_i^{j,+}, & i = 0 \\ f_i^{j-1,+}, & i = 1 \\ f_i^{j+1,+}, & i = -1 \end{cases} \quad (13)$$

where

$$f_i^{j,+} = f_i(x_j, t) - (\mathbf{M}^{-1} \mathbf{S} \mathbf{M})_{ik} (f_k(x_j, t) - f_k^{eq}(x_j, t)) + \delta_t [\mathbf{M}^{-1} (\mathbf{I} - \frac{\theta \mathbf{S}}{2}) \mathbf{M}]_{ik} R_k, i = 0, 1, -1. \quad (14)$$

After taking some manipulations of the evolution equation, as shown in Fig. 1 (see Appendix A for details), we can

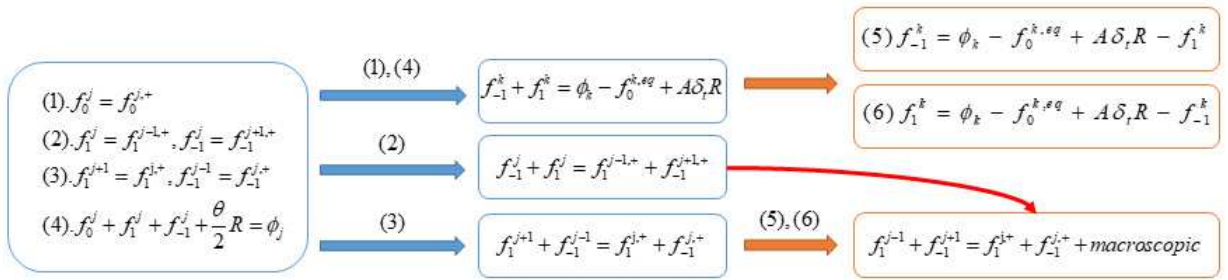


Figure 1: The operation process to get the equivalent finite-difference scheme.

obtain the following equivalent difference equation of the MRT model,

$$\frac{\phi_{k+1} u_{k+1} - \phi_{k-1} u_{k-1}}{2\delta x} = D \frac{\phi_{k+1} - 2\phi_k + \phi_{k-1}}{\delta x^2} + R, \quad (15)$$

where $D = (1/s_1 - 1/2)c_s^2\delta t$, $c_s^2 = 2\omega_1c^2$. Then we consider the D2Q9 MRT model for x-direction steady problems with constant R , and set the distribution function as $f_i^j = f_i(x_k, y_j)$, with y_j being a discrete grid point, and i being the direction of distribution function. Eq. (2) can be rewritten as

$$f_i^j = \begin{cases} f_i^{j,+}, & i = 0, 1, 3 \\ f_i^{j-1,+}, & i = 2, 5, 6 \\ f_i^{j+1,+}, & i = 4, 7, 8 \end{cases} \quad (16)$$

where $f_i^{j,+} = f_i(x_k, y_j, t)^+$ is the distribution function after collision. Then we can take a combination of distribution function as

$$f_{013}^k = f_{013}^k - (s_0 - s_2)(f_{478}^k - f_{478}^{k,eq}) - s_0(f_{013}^k - f_{013}^{k,eq}) - (s_0 - s_2)(f_{256}^k - f_{256}^{k,eq}) + [(\omega_1 + 2\omega_5)\theta(s_2 - s_0) + (\omega_0 + 2\omega_1)(1 - \frac{\theta s_0}{2})]\delta_t R, \quad (17a)$$

$$f_{256}^{k+1} = f_{256}^k - (\frac{s_2}{2} - \frac{s_1}{2})(f_{478}^k - f_{478}^{k,eq}) - (\frac{s_2}{2} + \frac{s_1}{2})(f_{256}^k - f_{256}^{k,eq}) + (\omega_1 + 2\omega_5)(1 - \frac{\theta s_2}{2})\delta_t R, \quad (17b)$$

$$f_{478}^{k-1} = f_{478}^k - (\frac{s_1}{2} + \frac{s_2}{2})(f_{478}^k - f_{478}^{k,eq}) - (\frac{s_2}{2} - \frac{s_1}{2})(f_{256}^k - f_{256}^{k,eq}) + (\omega_1 + 2\omega_5)(1 - \frac{\theta s_2}{2})\delta_t R, \quad (17c)$$

where $f_{ijm}^k = f_i^k + f_j^k + f_m^k$, $f_{ijm}^{k,eq} = f_i^{k,eq} + f_j^{k,eq} + f_m^{k,eq}$. According to Eq. (12), we can obtain

$$f_{013}^k = \phi_k - f_{256}^k - f_{478}^k - \frac{\theta R}{2}\delta t. \quad (18)$$

Substituting Eq. (18) into Eq. (17a), one can obtain

$$f_{256}^k + f_{478}^k = \phi_k - f_{013}^{k,eq} + A\delta_t R, \quad (19)$$

where $a_0 = \omega_0 + 2\omega_1$, $a_1 = \omega_1 + 2\omega_5$, $A = -(a_0 + a_1 s_2 \theta)/s_2$, with $\omega_1 = \omega_2 = \omega_3 = \omega_4$, $\omega_5 = \omega_6 = \omega_7 = \omega_8$. With the help of Eq. (19), we can rewritten Eqs. (17b) and (17c) as

$$f_{256}^{k+1} = (1 - s_1)f_{256}^k + s_1 f_{256}^{k,eq} + B\delta_t R, \quad (20a)$$

$$f_{478}^{k-1} = (1 - s_1)f_{478}^k + s_1 f_{478}^{k,eq} + B\delta_t R, \quad (20b)$$

where $B = a_1(1 - \theta s_2/2) - (s_2 - s_1)A/2$. Then we can get the following equation according to Eqs. (20a) and (20b)

$$f_{256}^k = (1 - s_1)f_{256}^{k-1} + s_1f_{256}^{k-1,eq} + B\delta_t R, \quad (21a)$$

$$f_{478}^k = (1 - s_1)f_{478}^{k+1} + s_1f_{478}^{k+1,eq} + B\delta_t R. \quad (21b)$$

With the help of Eq. (19), Eqs. (21a) and (21b) can be written as

$$f_{256}^k = (1 - s_1)(\phi_{k-1} - f_{478}^{k-1} - f_{013}^{k-1,eq} + A\delta_t R) + s_1f_{256}^{k-1,eq} + B\delta_t R, \quad (22a)$$

$$f_{478}^k = (1 - s_1)(\phi_{k+1} - f_{256}^{k+1} - f_{013}^{k+1,eq} + A\delta_t R) + s_1f_{478}^{k+1,eq} + B\delta_t R. \quad (22b)$$

Taking a sum of Eqs. (20a), (20b), (22a) and (22b), one can obtain

$$a_1 \frac{s_1 - 2}{s_1} (\phi_{k+1} + \phi_{k-1} - 2\phi_k) = \frac{\phi_{k+1}u_{y,k+1} - \phi_{k-1}u_{y,k-1}}{2c} + \delta_t R, \quad (23)$$

where Eq. (19) has been adopted. Then we can obtain the following equivalent difference equation of the MRT model,

$$\frac{\phi_{k+1}u_{y,k+1} - \phi_{k-1}u_{y,k-1}}{2\delta x} = D \frac{\phi_{k+1} - 2\phi_k + \phi_{k-1}}{\delta x^2} + R, \quad (24)$$

55 where $D = (1/s_1 - 1/2)c_s^2\delta t$, $c_s^2 = 2a_1c^2$, $a_1 = \omega_1 + 2\omega_5$. Here we would like to point out that if we adopt different transform matrix \mathbf{M} which is constructed by orthogonal vectors, one can obtain the same equivalent difference equation [35].

Actually, for higher dimensions lattice velocity models (e.g., D3Q27), one can obtain the similar difference scheme as Eq. (24) (see Appendix A for details). Then we will get a useful equation, in the following derivation. When $k = 1$, Eq. (21b) can be written as

$$f_{478}^1 = (1 - s_1)f_{478}^2 + s_1f_{478}^{2,eq} + B\delta_t R. \quad (25)$$

Substituting Eq. (19) into Eq. (25), one can obtain

$$f_{478}^1 = (1 - s_1)(\phi_2 - f_{013}^{2,eq} + A\delta_t R - f_{256}^2) + s_1f_{478}^{2,eq} + B\delta_t R. \quad (26)$$

In addition, substituting Eq. (22a) into Eq. (26) with the help of Eq. (3) gives rise to

$$f_{478}^1 = (1 - s_1)(2a_1\phi_2 + A\delta_t R - (1 - s_1)(2a_1\phi_1 - f_{478}^1 + A\delta_t R) + 2a_1s_1\phi_1 + B\delta_t R) + 2a_1s_1\phi_2 + B\delta_t R. \quad (27)$$

We can rewrite the Eq. (27) as

$$s_1 f_{478}^1 = a_1\phi_2 + (s_1 - 1)a_1\phi_1 + \frac{(s_1 A - B)(1 - s_1) + B}{2 - s_1} \delta_t R. \quad (28)$$

3.2. Discrete effect of the ABB boundary scheme

To simplify the analysis on the discrete effect of the ABB boundary scheme, a unidirectional and time-independent diffusion problem is adopted, and it can be described by the following simplified equation and boundary conditions for one dimensional problem

$$D \frac{\partial^2 \phi}{\partial x^2} + R = 0, \quad (29)$$

$$\phi(x = 0) = \phi_0, \phi(x = L) = \phi_L, \quad (30)$$

where ϕ_0 and ϕ_L are constant, L is the width and D is the diffusion coefficient. R is a constant source term, and is defined by

$$R = 2D \frac{\Delta \phi}{L^2}, \Delta \phi = \phi_L - \phi_0. \quad (31)$$

The analytical solution of the problem is given by

$$\phi(x) = \phi_0 + \frac{x}{L} \left(2 - \frac{x}{L}\right) \Delta \phi. \quad (32)$$

Based on Eq. (15), equivalent difference equation for the MRT model for Eq. (29),

$$D \frac{\phi_{k+1} - 2\phi_k + \phi_{k-1}}{\delta x^2} + R = 0. \quad (33)$$

Then we can obtain the solution of Eq. (33),

$$\phi_k = -\frac{\Delta \phi}{N^2} k^2 + ak + b, \quad (34)$$

where a, b are parameters to be determined. If we consider ABB scheme, the value of ϕ at bottom and top boundaries can be given by

$$\phi_{0.5} = \phi_0 + \phi_s^{0.5}, \quad \phi_{N+0.5} = \phi_L + \phi_s^{N+0.5}. \quad (35)$$

where $\phi_s^{0.5}$, $\phi_s^{N+0.5}$ are numerical slip caused by ABB scheme, N representing grid number. Substituting Eq. (35) into Eq. (34), we obtain the numerical solution

$$\phi_k = -\frac{\Delta\phi}{N^2}k^2 + (2N+1)\frac{\Delta\phi}{N^2}k - (4N+1)\frac{\Delta\phi}{4N^2} + (k-\frac{1}{2})\frac{\phi_s^{N+0.5} - \phi_s^{0.5}}{N} + \phi_0 + \phi_s^{0.5}, \quad (36)$$

In the following, we will focus on how to determine $\phi_s^{0.5}$ and $\phi_s^{N+0.5}$ from the ABB scheme. As Fig. 2 shown, the unknown distribution functions at the layers $k=1$, $k=N$ can be determined by the following equations [29],



Figure 2: The boundary arrangement in the D1Q3 lattice model; the black line denotes the boundary and is located at $k=1/2$ and $k=N+1/2$.

$$f_1^1 = -f_{-1}^{1,+} + 2\omega_1\phi_0, \quad (37)$$

$$f_{-1}^N = -f_1^{N,+} + 2\omega_1\phi_L, \quad (38)$$

where $f_{-1}^{1,+}$, $-f_1^{N,+}$ represent the distribution function after collision at the layers $k=1$ and $k=N$ respectively. Following the process in Appendix B, we can get the numerical slip,

$$\phi_s^{0.5} = \frac{4(2-s_1)\omega_0 + s_2[-4 + s_1 + 4(2-s_1)\omega_1\theta]}{4s_1s_2} \frac{\Delta\phi}{N^2}, \quad (39)$$

$$\phi_s^{N+0.5} = \frac{4(2-s_1)\omega_0 + s_2[-4 + s_1 + 4(2-s_1)\omega_1\theta]}{4s_1s_2} \frac{\Delta\phi}{N^2}. \quad (40)$$

As we can see, $\phi_s^{0.5}$ and $\phi_s^{N+0.5}$ have the same expression, thus we denote them by ϕ_s in the following discussion. If the free parameter s_2 is chosen to satisfy the relation,

$$4(2-s_1)\omega_0 + s_2[-4 + s_1 + 4(2-s_1)\omega_1\theta] = 0, \quad (41)$$

the discrete effect of the ABB scheme can be eliminated.

60 Furthermore, when we use the BGK model ($s_1 = s_2$) to deal with the problem, and take the weight coefficients ω_0 and ω_1 to satisfy Eq. (41), the discrete effect on the ABB boundary scheme can also be eliminated. However, this

selection of the weight coefficients in the BGK model is limited due to the fact that the weight coefficients should be greater than 0 and less than 1.

Similarly, for the two-dimensional unidirectional steady problem with a parabolic distribution in one direction, we analyze the discrete effect in D2Q9 MRT model. For the ABB scheme,

$$f_2^1 = -f_4^{1,+} + 2\omega_1\phi_0, \quad (42a)$$

$$f_5^1 = -f_7^{1,+} + 2\omega_5\phi_0, \quad (42b)$$

$$f_6^1 = -f_8^{1,+} + 2\omega_5\phi_0, \quad (42c)$$

where the $f_i^{1,+} = f_i(x_k, y_1, t)^+$ represent the distribution function after the collision. Taking a sum of Eqs. (42a), (42b), and (42c), we obtain

$$f_{256}^1 = -f_{478}^{1,+} + 2a_1\phi_0, \quad (43)$$

which can be written as

$$2a_1\phi_1 + A\delta tR = s_1f_{478}^1 - a_1s_1\phi_1 - B\delta tR + 2a_1\phi_0, \quad (44)$$

with the help of Eqs. (19) and (20b). Substituting

$$\phi_1 = \phi_0 + \phi_s + (2 - \frac{1}{2N})\frac{\Delta\phi}{2N}, \quad (45a)$$

$$\phi_2 = \phi_0 + \phi_s + (2 - \frac{3}{2N})\frac{3\Delta\phi}{2N}, \quad (45b)$$

and Eq. (28) into Eq. (44), we can obtain

$$\phi_s = \frac{2a_0\Delta\phi}{N^2} \left[\left(\frac{1}{s_1} - \frac{1}{2} \right) \left(\frac{1}{s_2} - \frac{1-2a_1\theta}{2a_0} \right) - \frac{1}{8a_0} \right], \quad (46)$$

where $a_0 = \omega_0 + 2\omega_1$, $a_1 = \omega_1 + 2\omega_5$ in D2Q9 model.

Similarly, for the three-dimensional unidirectional steady problem with a parabolic distribution in one direction, one can obtain the following results with a similar derivation process,

$$\phi_s = \frac{2a_0\Delta\phi}{N^2} \left[\left(\frac{1}{s_1} - \frac{1}{2} \right) \left(\frac{1}{s_2} - \frac{1-2a_1\theta}{2a_0} \right) - \frac{1}{8a_0} \right], \quad (47)$$

where $c_s^2 = 2a_1c^2$, $a_0 = \omega_0 + 4\omega_1 + 4\omega_7$, $a_1 = \omega_1 + 4\omega_7 + 4\omega_{19}$ in D3Q19 model. Taking the following equation

$$\left(\frac{1}{s_2} - \frac{(a_0 + 2a_1(1 - \theta))}{2a_0}\right)\left(\frac{1}{s_1} - \frac{1}{2}\right) = \frac{1}{8a_0}, \quad (48)$$

in Eq. (47), one can eliminate the discrete effect. The parameters a_0 and a_1 in the different lattice model are listed in Table 1, the velocities of D2Q9 and D3Q27 models are presented in Fig. 3, and the relaxation factors s_1 and s_2 are associated with first and second moments. We note that when $\theta = 1$, $\omega_i = 1/4(i = 1 - 4)$ in D2Q4 model, $\omega_i = 1/5(i = 0 - 4)$ in D2Q5 model, $\omega_0 = 4/9, \omega_{1-4} = 1/9, \omega_{5-8} = 1/36$ in D2Q9 model, Eq. (47) contains the previous works [30]. And Eq. (48) is consist with the recent results [31] when $\theta = 1$ in the frame of TRT model. It should be noted that for a specified lattice model, we can determine the explicit expression of ϕ_s from Eq. (47), but the numerical slip ϕ_s could not be eliminated since w_i is not flexible enough to satisfy Eq. (48). For example, in the D1Q2 model, ($\omega_0 = 0, \omega_1 = 1/2$), Eq. (48) can not be satisfied under the condition of $0 < s_1 < 2$ and $0 < s_2 < 2$.

Table 1: The a_0 and a_1 in different lattice models.

Different models	a_0	a_1
D1Q2	0	ω_1
D1Q3	ω_0	ω_1
D2Q4	$2\omega_1$	ω_1
D2Q5	$\omega_0 + 2\omega_1$	ω_1
D2Q9	$\omega_0 + 2\omega_1$	$\omega_1 + 2\omega_5$
D3Q7	$\omega_0 + 4\omega_1$	ω_1
D3Q13	$\omega_0 + 4\omega_1$	$4\omega_1$
D3Q15	$\omega_0 + 4\omega_1$	$\omega_1 + 4\omega_7$
D3Q19	$\omega_0 + 4\omega_1 + 4\omega_7$	$\omega_1 + 4\omega_7$
D3Q27	$\omega_0 + 4\omega_1 + 4\omega_7$	$\omega_1 + 4\omega_7 + 4\omega_{19}$

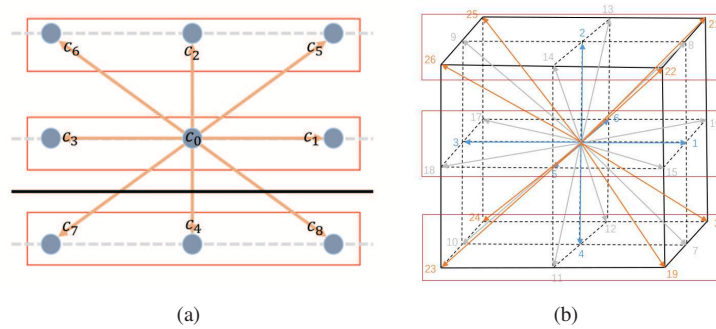


Figure 3: The Discrete velocity of D2Q9 and D3Q27, respectively.

3.3. Discrete effect of the BB boundary scheme

In this section, we analyze the BB boundary scheme under the same assumptions. For D2Q9 model with the BB boundary scheme [36],

$$f_2^0 = f_4^0, \quad (49a)$$

$$f_5^0 = f_7^0, \quad (49b)$$

$$f_6^0 = f_8^0. \quad (49c)$$

Summing Eqs. (49a), (49b), and (49c), one can obtain

$$f_{256}^0 = f_{478}^0. \quad (50)$$

Then Eq. (17b) can be written as

$$f_{256}^1 = f_{478}^0 - \left(\frac{s_2}{2} - \frac{s_1}{2}\right)(f_{478}^0 - f_{478}^{k,eq}) - \left(\frac{s_2}{2} + \frac{s_1}{2}\right)(f_{478}^0 - f_{256}^{k,eq}) + a_1\left(1 - \frac{\theta s_2}{2}\right)\delta_t R, \quad (51)$$

where $a_1 = \omega_1 + 2\omega_5$. One can obtain

$$2a_1 f_{478}^1 + AR - f_{478}^1 = (1 - s_2)[(1 - s_1)f_{478}^1 + s_1 a_1 \phi_1 + BR] + a_1 s_2 \phi_0 + a_1\left(1 - \frac{\theta s_2}{2}\right)\delta_t R. \quad (52)$$

with the help of Eqs. (19) and (20b). Substituting

$$\phi_1 = \phi_0 + \phi_s + \left(2 - \frac{1}{N}\right)\frac{\Delta\phi}{N}, \quad (53a)$$

$$\phi_2 = \phi_0 + \phi_s + \left(2 - \frac{2}{N}\right)\frac{2\Delta\phi}{N}, \quad (53b)$$

and Eq. (28) into Eq. (52), we can obtain

$$\phi_s = \frac{2(2 - s_1 - s_2)\Delta\phi}{s_1 s_2 N}. \quad (54)$$

3.4. Discrete effect of the NEE boundary scheme

For the NEE scheme [37],

$$f_k^0 = f_k^{0,eq} + (f_k^1 - f_k^{1,eq}), \quad (55)$$

Based on Eq. (55), we obtain

$$f_{256}^0 = f_{256}^{0,eq} + (f_{256}^1 - f_{256}^{1,eq}). \quad (56)$$

According to Eq. (21a), we have

$$f_{256}^1 = (1 - s_1)f_{256}^0 + s_1f_{256}^{0,eq} + B\delta_t R, \quad (57)$$

which can be written as

$$f_{256}^1 = (1 - s_1)(f_{256}^{0,eq} + (f_{256}^1 - f_{256}^{1,eq})) + s_1f_{256}^{0,eq} + B\delta_t R, \quad (58)$$

with the help of Eq. (56). Substituting Eq. (19) into Eq. (58), one can obtain

$$2a_1\phi_1 + A\delta_t R = s_1f_{478}^1 + (1 - s_1)(a_1\phi_0 + a_1\phi_1 + A\delta_t R) + a_1s_1\phi_0 + B\delta_t R. \quad (59)$$

Substituting

$$\phi_1 = \phi_0 + \phi_s + (2 - \frac{1}{N})\frac{\Delta\phi}{N}, \quad (60a)$$

$$\phi_2 = \phi_0 + \phi_s + (2 - \frac{2}{N})\frac{2\Delta\phi}{N}, \quad (60b)$$

and Eq. (28) into Eq. (59), one can obtain

$$\phi_s = \frac{2(1 - s_1)\Delta\phi}{s_1N^2}. \quad (61)$$

75 4. NUMERICAL RESULTS

In this section, some simulations of CDEs are performed to test above analysis, and ABB scheme is employed to treat the Dirichlet boundary conditions. In our simulations, the global relative error (GRE) and maximum error(E_{max}) are used to measure accuracy, and are defined as

$$GRE = \frac{\sqrt{\sum_i |\phi(\mathbf{x}_i, t) - \phi^*(\mathbf{x}_i, t)|^2}}{\sqrt{\sum_i |\phi^*(\mathbf{x}_i, t)|^2}}, \quad E_{max} = \max_i \{|\phi(\mathbf{x}_i, t) - \phi^*(\mathbf{x}_i, t)|\} \quad (62)$$

where ϕ and ϕ^* are the numerical and analytical solutions, respectively. In addition, the following convergent criterion for the steady problems is used,

$$\frac{\sqrt{\sum_i |\phi(\mathbf{x}_i, t+1) - \phi(\mathbf{x}_i, t)|^2}}{\sqrt{\sum_i |\phi(\mathbf{x}_i, t)|^2}} < 10^{-9}. \quad (63)$$

In our simulations, f_i^{eq} is applied to approximate the initial distribution function f_i .

4.1. Some unidirectional time-independent real-valued CDEs

4.1.1. A linear time-independent diffusion equation

We first consider a two-dimensional linear time-independent diffusion equation with a constant source term,

$$\begin{aligned} D \frac{\partial^2 \phi}{\partial y^2} + R &= 0, \\ \phi(x, y = 0) &= \phi_0, \quad \phi(x, y = L) = \phi_L, \end{aligned} \quad (64)$$

where ϕ_0 and ϕ_L are two constants, L is the width between the top and bottom boundaries, and R is the source term and is defined by

$$R = \frac{2D\Delta\phi}{L^2}, \Delta\phi = \phi_L - \phi_0. \quad (65)$$

The analytical solution of this problem is given by

$$\phi(x, y) = \phi_0 + \frac{y}{L} \left(2 - \frac{y}{L}\right) \Delta\phi. \quad (66)$$

Here we consider the popular D2Q9 MRT model with $\theta = 1$, the physical parameter $L = 1.0$, $u_x = 0.1$, $u_y = 0.0$, the diffusion coefficient $D = 0.1$, the boundary conditions $\phi_0 = 0$, $\phi_L = 1$, $\delta_x = L/N$ with the grid number N varying from 5 to 17.

First, we would like to verify that the parameters except s_1 and s_2 have little effect on numerical results. In our simulations, the value of s_1 is determined by the diffusion coefficient, while s_2 is given by Eq. (48). We measured the GREs of the problem under different values of s_3 , and present the results in Table 2 and Table 3. As shown in these table, for the fixed s_1 and N , the relaxation parameter s_3 has little influence on GREs. For this reason, except s_1 and s_2 , the other parameters in \mathbf{S} are set to be 1.0 in the following simulations. In general, the GRE decreases with the increase of grid number N , and as we shown in Table 2 the GRE increases for the accumulation of mechanical errors when the grid number N increases.

After that, we test different weight coefficients in the D2Q9 BGK model when $s_1 = 0.1$ and 0.5. In Fig. (4), the case 1 is $\omega_i = 1/9, (i = 0 - 8)$, the case 2 is $\omega_0 = 4/9, \omega_1 = 1/9, \omega_5 = 1/36$, the case 3 is a set of weight coefficients satisfied Eq. (48). In our simulation, case 3 is $\omega_0 = 1/1083, \omega_1 = 1/4332, \omega_5 = 1081/4332$ when $s_1 = 0.1$, $\omega_0 = 1/27, \omega_1 = 1/108, \omega_5 = 25/108$ when $s_1 = 0.5$. We can see that case 3 has more accurate results than case 1 and case 2. As we known, the weight coefficients in the D2Q9 model are given as $\omega_0 = 4/9, \omega_1 = 1/9, \omega_5 = 1/36$ for Navier-Stokes equations. Actually, weight coefficients in the LB model for CDEs are more flexible and they could be adjusted to give more accurate results. This adjustment has certain limitations because the weight coefficients must be greater than zero. For BGK model, taking $s_1 = s_2, 0 < a_0 < 1$, and $(1/s_1 - 1/2)^2 = 1/(8a_0)$,

Table 2: The GREs of D2Q9 MRT model with ABB boundary scheme and different relaxation parameters ($w_0 = 4/9, w_1 = 1/9, w_5 = 1/36$).

Different values		$N = 5$	$N = 9$	$N = 17$
$s_1 = 0.1$	$s_3 = 0.0$	1.6143×10^{-14}	1.1575×10^{-14}	4.6266×10^{-15}
	$s_3 = 1.0$	9.1778×10^{-16}	4.5187×10^{-16}	3.2051×10^{-16}
	$s_3 = s_1$	6.4495×10^{-16}	6.5046×10^{-16}	2.8975×10^{-16}
	$s_3 = s_2$	7.0977×10^{-16}	5.5918×10^{-16}	6.5757×10^{-16}
$s_1 = 0.6$	$s_3 = 0.0$	1.4288×10^{-14}	9.2039×10^{-15}	2.1330×10^{-8}
	$s_3 = 1.0$	4.8550×10^{-16}	2.4793×10^{-15}	2.1372×10^{-8}
	$s_3 = s_1$	2.6330×10^{-16}	1.5328×10^{-15}	2.1355×10^{-8}
	$s_3 = s_2$	4.5732×10^{-16}	4.3549×10^{-15}	2.1393×10^{-8}
$s_1 = 1.071797$	$s_3 = 0.0$	2.1428×10^{-14}	1.8222×10^{-8}	1.1939×10^{-7}
	$s_3 = 1.0$	2.5713×10^{-15}	1.8272×10^{-8}	1.1947×10^{-7}
	$s_3 = s_1$	2.3383×10^{-15}	1.8275×10^{-8}	1.1948×10^{-7}
	$s_3 = s_2$	2.2578×10^{-15}	1.8275×10^{-8}	1.1948×10^{-7}
$s_1 = 1.9$	$s_3 = 0.0$	2.2912×10^{-7}	8.1846×10^{-7}	3.0786×10^{-6}
	$s_3 = 1.0$	2.2926×10^{-7}	8.1861×10^{-7}	3.0787×10^{-6}
	$s_3 = s_1$	2.2938×10^{-7}	8.1873×10^{-7}	3.0789×10^{-6}
	$s_3 = s_2$	2.2914×10^{-7}	8.1849×10^{-7}	3.0786×10^{-6}

then we can get the limitation $1/s_1 > (1 + \sqrt{2})/2\sqrt{2}$. When $1/s_1 > (1 + \sqrt{2})/2\sqrt{2}$, ϕ_s on ABB boundary scheme can be eliminated with the adjustment of the weight coefficients in BGK model. As for BB and NEE boundary schemes, when we consider BGK model(that is $s_1 = s_2$), ϕ_s can be eliminated only if $s_1 = 1$. For this reason, the adjustment of ABB scheme is more flexible.

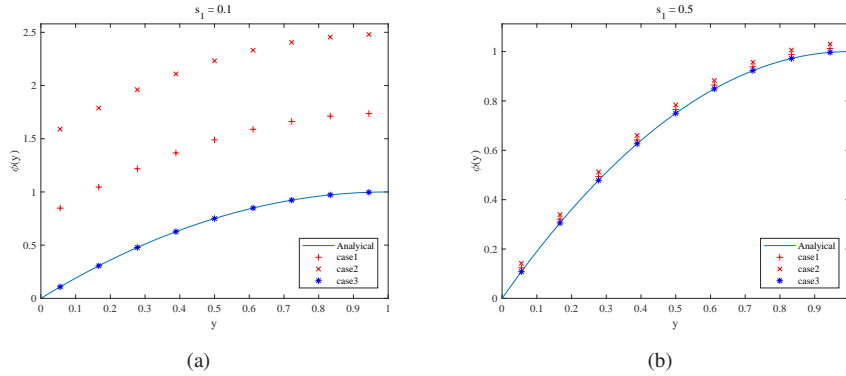


Figure 4: (Color online) D3Q19 BGK models with ABB boundary condition and the different weight coefficients.

100

ϕ_s of ABB boundary scheme depends on s_1, s_2, θ and c_s^2 , ϕ_s of BB boundary scheme depends on s_1 and s_2 , and ϕ_s of NEE scheme only depends on s_1 . We test the same problem with NEE scheme, taking $s_1 = 0.6, 1.2, 1.9$, with different s_2 . As we shown in Fig. (5), s_2 has little effect on numerical results. And when we change the value of s_1 , we can see that the GRE has a minimum when $s_1 = 1$, which agree with Eq. (61). Then we consider ϕ_s of BB scheme as Eq. (54). When $s_2 = 2 - s_1$, the discrete effect can be eliminated for the unidirectional steady problem

105

Table 3: The E_{max} of D2Q9 MRT model with ABB boundary scheme and different relaxation parameters ($w_0 = 4/9, w_1 = 1/9, w_5 = 1/36$).

Different values		$N = 5$	$N = 9$	$N = 17$
$s_1 = 0.1$	$s_3 = 0.0$	2.1427×10^{-14}	1.5488×10^{-14}	4.6266×10^{-15}
	$s_3 = 1.0$	1.3322×10^{-16}	5.6899×10^{-16}	4.4409×10^{-16}
	$s_3 = s_1$	7.7716×10^{-16}	7.7716×10^{-16}	4.4409×10^{-16}
	$s_3 = s_2$	7.7716×10^{-16}	7.7716×10^{-16}	4.4409×10^{-16}
$s_1 = 0.6$	$s_3 = 0.0$	1.7097×10^{-14}	1.0214×10^{-15}	2.2029×10^{-8}
	$s_3 = 1.0$	4.4409×10^{-16}	2.5535×10^{-15}	2.2073×10^{-8}
	$s_3 = s_1$	3.3307×10^{-16}	1.6653×10^{-15}	2.2055×10^{-8}
	$s_3 = s_2$	4.4409×10^{-16}	4.6629×10^{-15}	2.2095×10^{-8}
$s_1 = 1.071797$	$s_3 = 0.0$	2.2759×10^{-14}	1.8820×10^{-8}	1.2330×10^{-7}
	$s_3 = 1.0$	2.4425×10^{-15}	1.8871×10^{-8}	1.2339×10^{-7}
	$s_3 = s_1$	2.2204×10^{-15}	1.8875×10^{-8}	1.2339×10^{-7}
	$s_3 = s_2$	2.2204×10^{-15}	1.8875×10^{-8}	1.2339×10^{-7}
$s_1 = 1.9$	$s_3 = 0.0$	2.3665×10^{-7}	8.4530×10^{-7}	3.1796×10^{-6}
	$s_3 = 1.0$	2.3679×10^{-7}	8.4546×10^{-7}	3.1797×10^{-6}
	$s_3 = s_1$	2.3691×10^{-7}	8.4558×10^{-7}	3.1798×10^{-6}
	$s_3 = s_2$	2.3667×10^{-7}	8.4534×10^{-7}	3.1796×10^{-6}

with a parabolic distribution in one direction. We take a simulation of the same problem as Eq. (64) with BB scheme, taking $s_1 = 0.1, 0.6, 1.0, 1.9$ respectively, and shown the result in Fig. (7). Under the same lattice size to eliminate the numerical slip in MRT model, we can adjust the parameter s_2 to satisfy $s_1 + s_2 = 2$ for BB boundary scheme while in the BGK model s_2 is determined by diffusion coefficient, and can not be adjusted. As the figures shown, we can adjust s_2 to get more accurate results.

Then, we consider a three-dimensional linear time-independent diffusion equation with a constant source term,

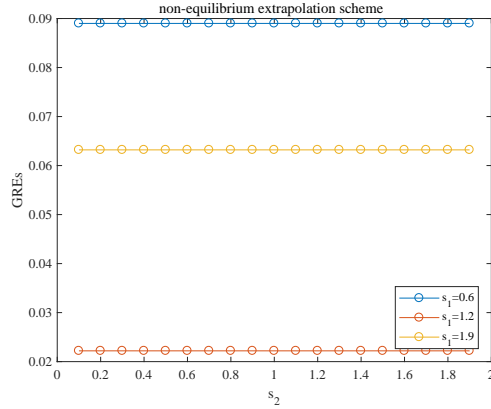
$$D \frac{\partial^2 \phi}{\partial z^2} + R = 0, \tag{67}$$

$$\phi(x, y, z = 0) = \phi_0, \quad \phi(x, y, z = L) = \phi_L.$$

The analytical solution of this problem is given by

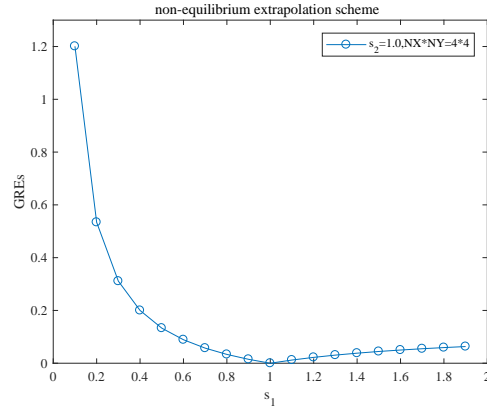
$$\phi(x, y, z) = \phi_0 + \frac{z}{L} \left(2 - \frac{z}{L}\right) \Delta \phi. \tag{68}$$

Here we consider the popular D3Q19 BGK and MRT model, the physical parameters $L = 1.0, u_x = 0.1, u_y = 0.0, u_z = 0.0$, the diffusion coefficient $D = 0.1$, the boundary conditions $\phi_0 = 0, \phi_L = 1, \delta_x = L/N$ with the grid number N varying from 5 to 17. For the ABB boundary scheme, we can adjust the parameter s_2 to satisfy Eq. (48) to get more accurate results. We perform some simulations with both BGK and MRT models, and present the results in Figs. 8, 9, 10 and 11. In these figures, the values of s_1 are taken to be 0.1, 0.6, 1.9, and a particular value satisfying Eq. (48)



(a)

Figure 5: (Color online) D2Q9 MRT models with NEE boundary scheme.



(a)

Figure 6: (Color online) D2Q9 MRT models with NEE boundary scheme.

under the condition of $s_1 = s_2$. From the results in Figs. 8, 9, 10 and 11, one can see that when s_2 satisfies Eq. (48), the numerical results are in good agreement with analytical solutions.

Here we give some comparisons of the GRE and E_{max} among D2Q5 and D2D9, D3Q7 and D3Q19 models in Tables. 4, 5, 6 and 7, and find that there are no apparent differences among D2Q5 and D2D9, D3Q7 and D3Q19 models when we adjust s_2 to satisfy Eq. (48) for ABB boundary scheme. However, the D2Q5 and D3Q7 models are more efficient since less discrete velocities are included.

4.1.2. Helmholtz equation

We also considered the following linear Helmholtz equation, as

$$\frac{\partial \phi}{\partial t} = \nabla^2 \phi - (\lambda^2 + \mu^2) \phi, \quad (69)$$

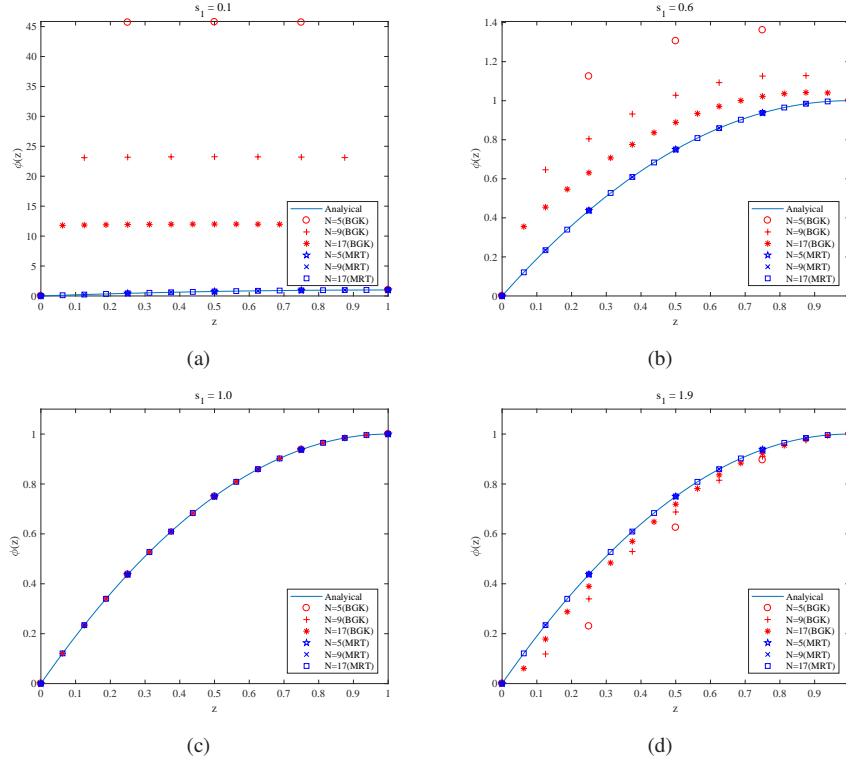


Figure 7: (Color online) D2Q9 BGK and MRT models with BB boundary scheme and the weight coefficients $\omega_0 = 4/9$, $\omega_1 = 1/9$, $\omega_7 = 1/36$.

with the boundary conditions

$$\begin{aligned}
 \phi &= 0, & 0 < x < H, & \quad y = H, \\
 \phi &= e^{-\lambda x}, & 0 < x < H, & \quad y = 0, \\
 \phi &= \frac{\sinh[\mu(1-y)]}{\sinh(\mu)}, & 0 < y < H, & \quad x = 0, \\
 \lambda\phi + \frac{\partial\phi}{\partial x} &= 0, & 0 < y < H, & \quad x = H.
 \end{aligned} \tag{70}$$

The physical domain is $\Omega = [0, H] \times [0, H]$, λ and μ are two constants. Under above conditions, steady analytical solution of Eq. (69) can be obtained

$$\phi^*(x, y) = e^{-\lambda x} \frac{\sinh[\mu(1-y)]}{\sinh(\mu)}, \tag{71}$$

which is more complicated than Eq. (64). We conducted some simulations with $\lambda = 0$ and $\mu = 1.0$, and present the results of D2Q9 MRT model under different values of s_1 in Figs. 12, 13, 14, where different weight coefficients are used. As we can see, the analytical solution Eq. (71) is time-independent and only depends on y when $\lambda = 0$ and $\mu = 1.0$. As shown in these figures, the relaxation parameter s_2 has a significant effect on numerical results, what is more, we can obtain the most accurate results when the value of s_2 determined by Eq. (48) is adopted.

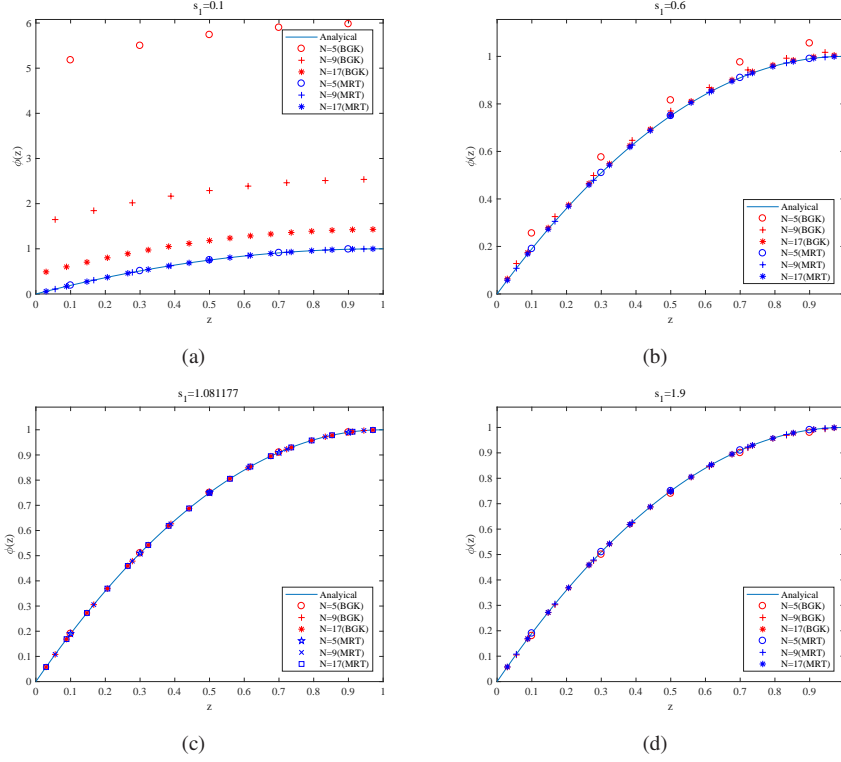


Figure 8: (Color online) D3Q19 BGK and MRT models with ABB boundary scheme and the weight coefficients $\omega_0 = 16/52, \omega_1 = 4/52, \omega_7 = 1/52$.

4.2. A unidirectional time-independent complex-valued CDEs

In this part, we further considered a simple two-dimension complex-valued problem governed by Eq. (64) to verify Eqs. (48) and (54) where $D = 1 + i, R = 4i, L = 1.0, u_x = 0.1, u_y = 0.0$, and the boundary conditions $\phi_0 = 0, \phi_L = 1 + i$. In our simulations, $\delta_x = L/N$ with the grid number N varying from 5 to 17, the D2Q5 MRT model ($\theta = 0$) is used.

The τ_r, τ_i are the relaxation times of the real and the imaginary parts respectively, and $S_r = \text{diag}(s_0, s_{r1}, s_{r1}, s_{r2}, s_{r2})$ and $S_i = \text{diag}(s_0, s_{i1}, s_{i1}, s_{i2}, s_{i2})$ are the diagonal relaxation matrix. Then we have [38]

$$\tau_r = \frac{D_r}{c_s^2 \Delta t} + \frac{1}{2}, \quad \tau_i = \frac{D_i}{c_s^2 \Delta t}, \quad s_{r1} = \frac{\tau_r}{\tau_r^2 + \tau_i^2}, \quad s_{i1} = -\frac{\tau_i}{\tau_r^2 + \tau_i^2}. \quad (72)$$

where $D = D_r + iD_i$. In our simulations, we take $s_0 = 0.0, s_{r1} = 1.0, 10.0, 0.501$, and s_{i1} is determined by Eq. (72). Substituting $s_1 = s_{r1} + is_{i1}$ and $s_2 = s_{r2} + is_{i2}$ into Eq. (48), we have

$$s_{r2}[-4 + s_{r1} + 4(2 - s_{r1})a_1\theta] - s_{i2}s_{i1}(1 - 4a_1\theta) + 4(2 - s_{r1})a_0 = 0, \quad (73)$$

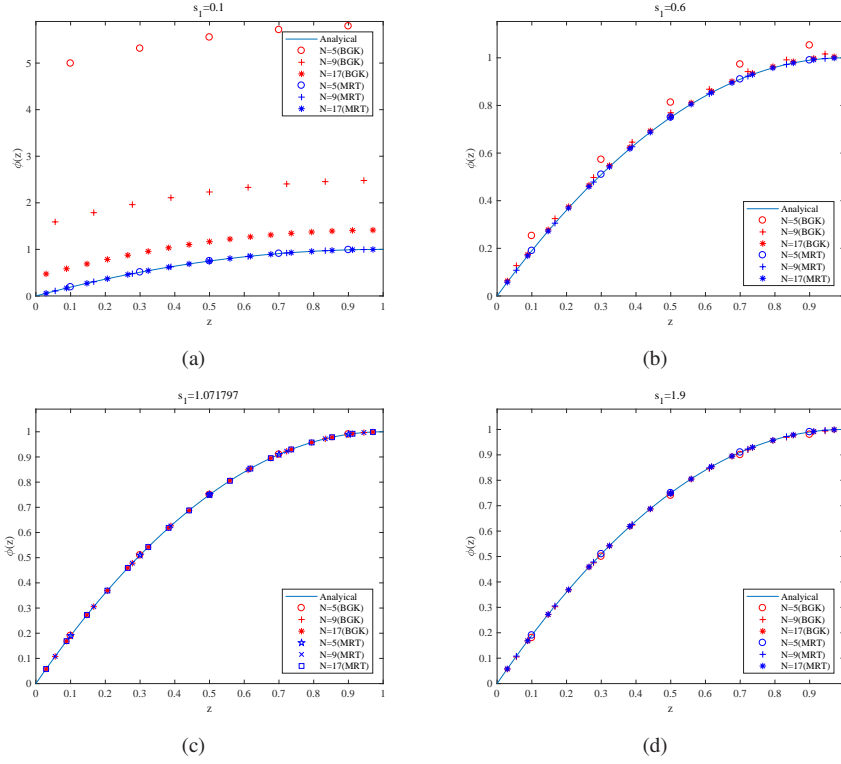


Figure 9: (Color online) D3Q19 BGK and MRT models with ABB boundary scheme and the weight coefficients $\omega_0 = 1/4$, $\omega_1 = 1/12$, $\omega_7 = 1/48$.

$$s_{i2}[-4 + s_{r1} + 4(2 - s_{r1})a_1\theta] + s_{r2}s_{i1}(1 - 4a_1\theta) - a_0s_{i1} = 0, \quad (74)$$

where $a_0 = \omega_0 + 2\omega_1$, $a_1 = \omega_1$ in the D2Q5 model. The s_{r2} and s_{i2} are choose to satisfy Eqs. (73) and (74), and it shows a good accuracy in Tables. 8 and 9. Then we take the same simulation with BB boundary scheme. s_2 is satisfied $s_1 + s_2 = 2$, that is $s_{r2} = 2 - s_{r1}$, $s_{i2} = -s_{r1}$ and shows the results in Tables. 10 and 11 which have good agreement with analytical solutions.

5. CONCLUSIONS

In this work, we performed a detailed analysis on the discrete effects of ABB, BB and NEE schemes of the popular one- to three- dimensional $DnQq$ MRT LB model for real- and complex-valued CDEs. Firstly, through the analysis with ABB boundary scheme, we obtain a relation with four adjustable parameters the weight coefficient, the relaxation factors s_1 and s_2 associated with first and second moments and a model parameter θ , which can be used to eliminate the discrete effect. We would also like to point out that taking $\theta = 1$ under some assumption, the relation in [31] in the framework of TRT model would be the special case of Eq. (48). The weight coefficient ω can be considered as an adjustable parameter makes the general relation Eq. (48) more flexible. Then we analyse the

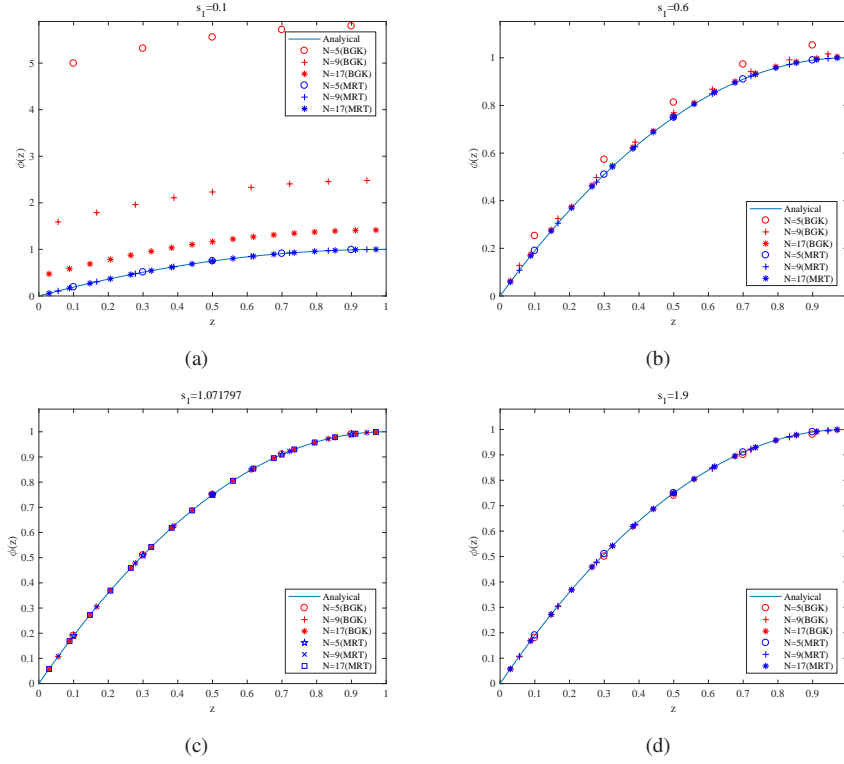


Figure 10: (Color online) D3Q19 BGK and MRT models with ABB boundary scheme and the weight coefficients $\omega_0 = 1/3, \omega_1 = 1/18, \omega_7 = 1/36$.

145 discrete effects of BB and NEE boundary schemes and indicate that the discrete effect of BB scheme can be eliminated when $s_1 + s_2 = 2$, and the discrete effect of NEE scheme can not be eliminated except $s_1 = 1$. The adjustment of ABB boundary scheme is more flexible than BB and NEE boundary schemes. We also carried out some numerical simulations of several special equations, including the real-valued linear time-independent diffusion equations in two- and three-dimensional space, the real-valued two-dimensional Helmholtz equation, and the complex-valued linear
 150 time-independent diffusion equation. The results also show that when the relation Eq. (48) for ABB boundary scheme and $s_1 + s_2 = 2$ for BB boundary scheme is satisfied, the discrete effect (or numerical slip) can be eliminated.

Acknowledgements

This work is supported by the National Natural Science Foundation of China (Grants No. 51576079 and No. 51836003), and the National Key Research and Development Program of China (Grant No. 2017YFE0100100)

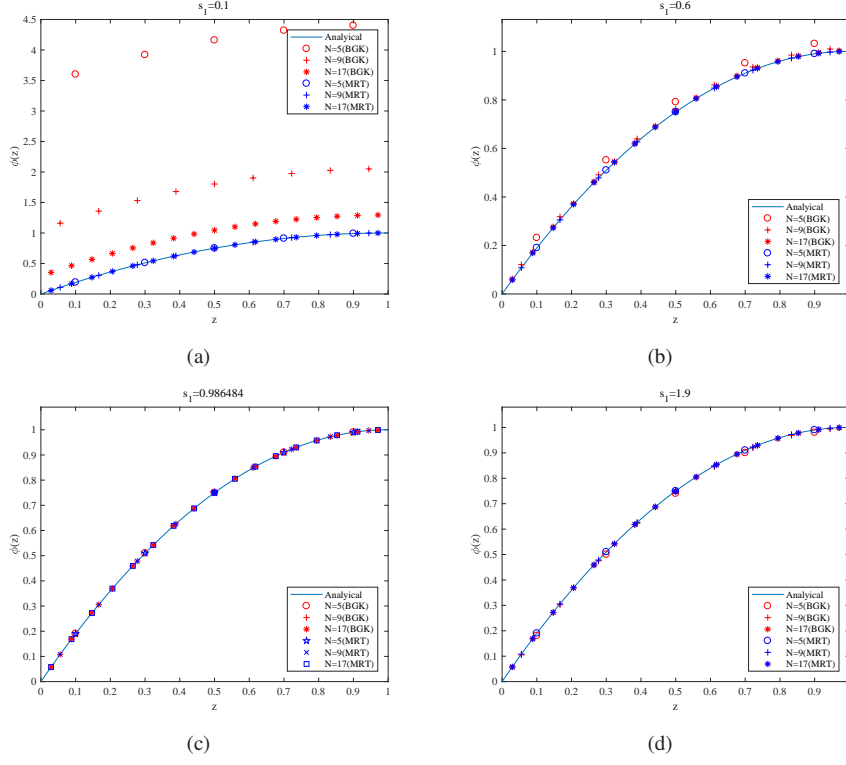


Figure 11: (Color online) D3Q19 BGK and MRT models with ABB boundary scheme and the weight coefficients $\omega_0 = 1/19, (i = 0 - 18)$.

156 APPENDIX

5.1. Equivalent difference equation of the MRT model

In this Appendix, we show how to derive the equivalent difference equation. Firstly, for the D1Q3 MRT model, from Eq. (13), we can obtain the expressions of the distribution functions,

$$f_{-1}^{k-1} = f_{-1}^k - \left(\frac{S_1}{2} + \frac{S_2}{2}\right)(f_{-1}^k - f_{-1}^{k,eq}) - \left(\frac{S_2}{2} - \frac{S_1}{2}\right)(f_1^k - f_1^{k,eq}) + w_1\left(1 - \frac{\theta s_2}{2}\right)\delta_t R, \quad (75a)$$

$$f_0^k = f_0^k - (s_0 - s_2)(f_{-1}^k - f_{-1}^{k,eq}) - s_0(f_0^k - f_0^{k,eq}) - (s_0 - s_2)(f_1^k - f_1^{k,eq}) + [w_1\theta(s_2 - s_0) + w_0\left(1 - \frac{\theta s_0}{2}\right)]\delta_t R, \quad (75b)$$

$$f_1^{k+1} = f_1^k - \left(\frac{S_2}{2} - \frac{S_1}{2}\right)(f_{-1}^k - f_{-1}^{k,eq}) - \left(\frac{S_2}{2} + \frac{S_1}{2}\right)(f_1^k - f_1^{k,eq}) + w_1\left(1 - \frac{\theta s_2}{2}\right)\delta_t R, \quad (75c)$$

where $f_i^k, f_i^{k,eq}$ are the distribution function and its equilibrium part at $x = k\delta_x$. According to Eqs. (12) and (3), we have

$$\phi_k = f_{-1}^k + f_0^k + f_1^k + \frac{\theta R}{2}\delta_t, \quad (76)$$

Table 4: The GREs of D2Q5 and D2Q9 MRT models with ABB boundary scheme and different parameters.

Different models		$N = 5$	$N = 9$	$N = 17$
$s_1 = 0.1$	$D2Q9, \omega_0 = \frac{4}{9}, \omega_1 = \frac{1}{9}, \omega_5 = \frac{1}{36}$	9.1778×10^{-16}	4.5187×10^{-16}	3.2051×10^{-16}
	$D2Q5, \omega_0 = \frac{1}{5}, \omega_1 = \frac{1}{5}$	5.7786×10^{-16}	5.2053×10^{-16}	3.3281×10^{-16}
$s_1 = 0.6$	$D2Q9, \omega_0 = \frac{4}{9}, \omega_1 = \frac{1}{9}, \omega_5 = \frac{1}{36}$	4.8550×10^{-16}	2.4793×10^{-15}	2.1372×10^{-8}
	$D2Q5, \omega_0 = \frac{1}{5}, \omega_1 = \frac{1}{5}$	2.8491×10^{-16}	1.5632×10^{-16}	1.5599×10^{-8}
$s_1 = 1.9$	$D2Q9, \omega_0 = \frac{4}{9}, \omega_1 = \frac{1}{9}, \omega_5 = \frac{1}{36}$	2.2926×10^{-7}	8.1861×10^{-7}	3.0787×10^{-6}
	$D2Q5, \omega_0 = \frac{1}{5}, \omega_1 = \frac{1}{5}$	1.4640×10^{-7}	6.7983×10^{-7}	2.6060×10^{-6}

Table 5: The E_{max} of D2Q5 and D2Q9 MRT models with ABB boundary scheme and different parameters.

Different models		$N = 5$	$N = 9$	$N = 17$
$s_1 = 0.1$	$D2Q9, \omega_0 = \frac{4}{9}, \omega_1 = \frac{1}{9}, \omega_5 = \frac{1}{36}$	1.3322×10^{-15}	5.6899×10^{-16}	4.4409×10^{-16}
	$D2Q5, \omega_0 = \frac{1}{5}, \omega_1 = \frac{1}{5}$	6.1062×10^{-16}	5.5511×10^{-16}	4.4409×10^{-16}
$s_1 = 0.6$	$D2Q9, \omega_0 = \frac{4}{9}, \omega_1 = \frac{1}{9}, \omega_5 = \frac{1}{36}$	4.4409×10^{-16}	2.5535×10^{-15}	2.2073×10^{-8}
	$D2Q5, \omega_0 = \frac{1}{5}, \omega_1 = \frac{1}{5}$	3.3307×10^{-16}	2.2204×10^{-16}	1.6110×10^{-8}
$s_1 = 1.9$	$D2Q9, \omega_0 = \frac{4}{9}, \omega_1 = \frac{1}{9}, \omega_5 = \frac{1}{36}$	2.3679×10^{-7}	8.4546×10^{-7}	3.1797×10^{-6}
	$D2Q5, \omega_0 = \frac{1}{5}, \omega_1 = \frac{1}{5}$	1.5121×10^{-7}	7.0213×10^{-7}	2.5966×10^{-6}

$$f_0^{k,eq} = \omega_0 \phi_k, \quad f_1^{k,eq} = \omega_1 \phi_k + \frac{u_k \phi_k}{2c}, \quad f_{-1}^{k,eq} = \omega_1 \phi_k - \frac{u_k \phi_k}{2c}. \quad (77)$$

Substituting Eq. (76) into Eq. (75b), one can obtain

$$f_{-1}^k + f_1^k = \phi_k - f_0^{k,eq} + A \delta_t R, \quad A = -\frac{\theta}{2} - \frac{s_2 - s_0}{s_2} \theta \left(\omega_1 - \frac{1}{2} \right) - \omega_0 \left(\frac{1}{s_2} - \frac{\theta s_0}{2s_2} \right). \quad (78)$$

Based on Eq. (78), we can get

$$f_{-1}^k = \phi_k - f_0^{k,eq} + A \delta_t R - f_1^k, \quad (79a)$$

$$f_1^k = \phi_k - f_0^{k,eq} + A \delta_t R - f_{-1}^k. \quad (79b)$$

Substituting Eq. (79a) into Eq. (75c), and with the help of Eq. (78), we have

$$f_1^{k+1} = (1 - s_1) f_1^k + s_1 f_1^{k,eq} + B \delta_t R, \quad B = \omega_1 \left(1 - \frac{\theta s_2}{2} \right) - \left(\frac{s_2}{2} - \frac{s_1}{2} \right) A. \quad (80)$$

Similarly, substituting Eq. (79b) into Eq. (75a), and with the aid of Eq. (78), one can obtain

$$f_{-1}^{k-1} = (1 - s_1) f_{-1}^k + s_1 f_{-1}^{k,eq} + B \delta_t R. \quad (81)$$

Table 6: The GREs of D3Q7 and D3Q19 MRT models with ABB boundary scheme and different parameters.

Different models	$N = 5$	$N = 9$	$N = 17$	
$s_1 = 0.1$	$D3Q19, \omega_0 = \frac{1}{3}, \omega_1 = \frac{1}{18}, \omega_7 = \frac{1}{36}$ $D3Q7, \omega_0 = \frac{1}{3}, \omega_1 = \frac{1}{9}$	3.0474×10^{-10} 1.5758×10^{-10}	1.7407×10^{-10} 7.4854×10^{-11}	1.9787×10^{-10} 5.6273×10^{-11}
$s_1 = 0.6$	$D3Q19, \omega_0 = \frac{1}{3}, \omega_1 = \frac{1}{18}, \omega_7 = \frac{1}{36}$ $D3Q7, \omega_0 = \frac{1}{3}, \omega_1 = \frac{1}{9}$	3.2280×10^{-9} 4.4101×10^{-11}	1.7372×10^{-9} 2.4137×10^{-9}	2.1372×10^{-8} 8.7858×10^{-8}
$s_1 = 1.9$	$D3Q19, \omega_0 = \frac{1}{3}, \omega_1 = \frac{1}{18}, \omega_7 = \frac{1}{36}$ $D3Q7, \omega_0 = \frac{1}{3}, \omega_1 = \frac{1}{9}$	2.2926×10^{-7} 3.1045×10^{-7}	8.1861×10^{-7} 1.2000×10^{-6}	3.0787×10^{-6} 4.6762×10^{-6}

Table 7: The E_{max} of D3Q7 and D3Q19 MRT models with ABB boundary scheme and different parameters.

Different models	$N = 5$	$N = 9$	$N = 17$	
$s_1 = 0.1$	$D3Q19, \omega_0 = \frac{1}{3}, \omega_1 = \frac{1}{18}, \omega_7 = \frac{1}{36}$ $D3Q7, \omega_0 = \frac{1}{3}, \omega_1 = \frac{1}{9}$	3.7204×10^{-10} 1.2115×10^{-10}	1.7549×10^{-10} 1.1272×10^{-11}	3.1573×10^{-10} 6.4008×10^{-11}
$s_1 = 0.6$	$D3Q19, \omega_0 = \frac{1}{3}, \omega_1 = \frac{1}{18}, \omega_7 = \frac{1}{36}$ $D3Q7, \omega_0 = \frac{1}{3}, \omega_1 = \frac{1}{9}$	3.3340×10^{-9} 4.5550×10^{-11}	1.7942×10^{-9} 2.4929×10^{-9}	2.2073×10^{-8} 9.0739×10^{-8}
$s_1 = 1.9$	$D3Q19, \omega_0 = \frac{1}{3}, \omega_1 = \frac{1}{18}, \omega_7 = \frac{1}{36}$ $D3Q7, \omega_0 = \frac{1}{3}, \omega_1 = \frac{1}{9}$	2.3679×10^{-7} 3.2065×10^{-7}	8.4546×10^{-7} 1.2394×10^{-6}	3.1797×10^{-6} 4.8296×10^{-6}

In addition, from Eqs. (80) and (81), we also have

$$f_1^k = (1 - s_1)f_1^{k-1} + s_1f_1^{k-1,eq} + B\delta_t R, \quad (82a)$$

$$f_{-1}^k = (1 - s_1)f_{-1}^{k+1} + s_1f_{-1}^{k+1,eq} + B\delta_t R. \quad (82b)$$

Summing Eqs. (82a) and (82b), one can derive the following equation,

$$\begin{aligned} f_1^k + f_{-1}^k = & (1 - s_1)[2\omega_1(\phi_{k+1} + \phi_{k-1}) - s_1(f_{-1}^{k,eq} + f_1^{k,eq}) - (1 - s_1)(f_1^k + f_{-1}^k) + 2(A - B)\delta_t R] \\ & + s_1(f_{-1}^{k+1,eq} + f_1^{k-1,eq}) + 2B\delta_t R, \end{aligned} \quad (83)$$

where Eqs. (80) and (81) have been used. Substituting Eq. (78) into Eq. (83) yields

$$\omega_1 \frac{s_1 - 2}{s_1} (\phi_{k+1} + \phi_{k-1} - 2\phi_k) = \frac{\phi_{k+1}u_{k+1} - \phi_{k-1}u_{k-1}}{2c} + \delta_t R, \quad (84)$$

where Eq. (77) has been adopted. From Eq. (84), we can obtain the equivalent difference equation of the MRT model, i.e., Eq. (15).

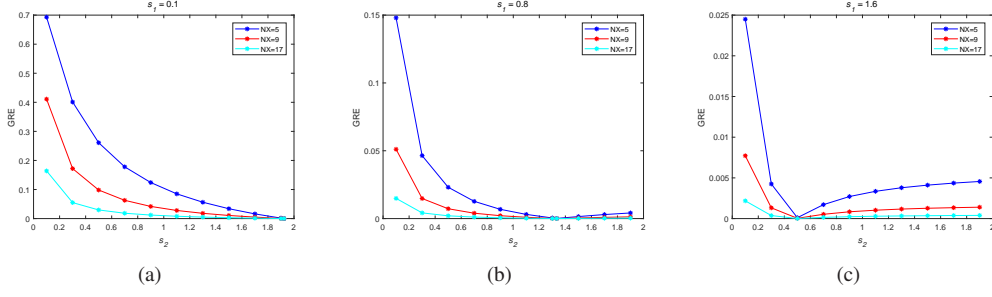


Figure 12: (Color online) The GREs of D2Q9 MRT model with ABB boundary scheme and weight coefficient $\omega_0 = 4/9$, $\omega_1 = 1/9$, $\omega_5 = 1/36$.

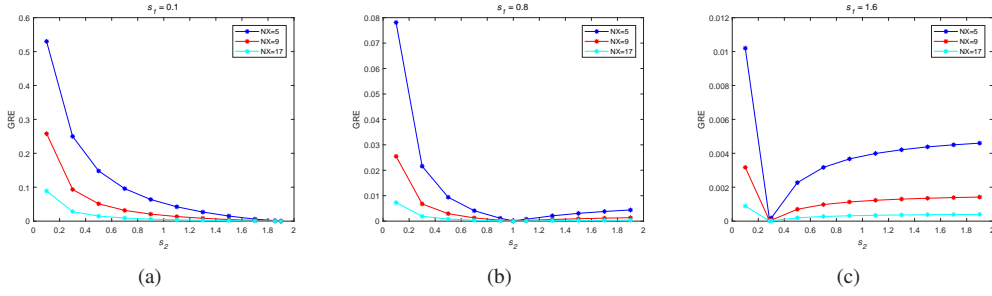


Figure 13: (Color online) The GREs of D2Q9 MRT model with ABB boundary scheme and weight coefficient $\omega_0 = 1/9$, $\omega_1 = 1/9$, $\omega_5 = 1/9$.

For the D3Q27 model, we have

$$\begin{aligned}
 f_{4,7,10,11,12,19,20,23,24}^{k-1} &= f_{4,7,10,11,12,19,20,23,24}^k - \left(\frac{s_1}{2} + \frac{s_2}{2}\right)(f_{4,7,10,11,12,19,20,23,24}^k - f_{4,7,10,11,12,19,20,23,24}^{k,eq}) \\
 &\quad - \left(\frac{s_2}{2} - \frac{s_1}{2}\right)(f_{2,8,9,13,14,21,22,25,26}^k - f_{2,8,9,13,14,21,22,25,26}^{k,eq}) + (\omega_1 + 2\omega_5)\left(1 - \frac{\theta s_2}{2}\right)\delta_t R,
 \end{aligned} \tag{85a}$$

$$\begin{aligned}
 f_{0,1,3,5,6,15,16,17,18}^k &= f_{0,1,3,5,6,15,16,17,18}^k - (s_0 - s_2)(f_{4,7,10,11,12,19,20,23,24}^k - f_{4,7,10,11,12,19,20,23,24}^{k,eq}) \\
 &\quad - s_0(f_{013}^k - f_{013}^{k,eq}) - (s_0 - s_2)(f_{2,8,9,13,14,21,22,25,26}^k - f_{2,8,9,13,14,21,22,25,26}^{k,eq}) \\
 &\quad + [(\omega_1 + 2\omega_5)\theta(s_2 - s_0) + (\omega_0 + 2\omega_1)\left(1 - \frac{\theta s_0}{2}\right)]\delta_t R,
 \end{aligned} \tag{85b}$$

$$\begin{aligned}
 f_{2,8,9,13,14,21,22,25,26}^{k+1} &= f_{2,8,9,13,14,21,22,25,26}^k - \left(\frac{s_2}{2} - \frac{s_1}{2}\right)(f_{4,7,10,11,12,19,20,23,24}^k - f_{4,7,10,11,12,19,20,23,24}^{k,eq}) \\
 &\quad - \left(\frac{s_2}{2} + \frac{s_1}{2}\right)(f_{2,8,9,13,14,21,22,25,26}^k - f_{2,8,9,13,14,21,22,25,26}^{k,eq}) + (\omega_1 + 2\omega_5)\left(1 - \frac{\theta s_2}{2}\right)\delta_t R,
 \end{aligned} \tag{85c}$$

where $f_{i,j,m}^k = f_i^k + f_j^k + f_m^k$, $f_{i,j,m}^{k,eq} = f_i^{k,eq} + f_j^{k,eq} + f_m^{k,eq}$. If the parts of $f_{0,1,3,5,6,15,16,17,18}^k$, $f_{2,8,9,13,14,21,22,25,26}^k$, and $f_{4,7,10,11,12,19,20,23,24}^k$ in the D3Q27 model are viewed as f_0^k , f_1^k , and f_{-1}^k in the D1Q3 model, $w_0 + 4w_1 + 4w_7$ and $w_1 + 4w_7 + 4w_{19}$ in the D3Q27 model are considered as w_0 and w_1 in D1Q3 model, we can derive the equivalent different Eq. (15) through the similar process.

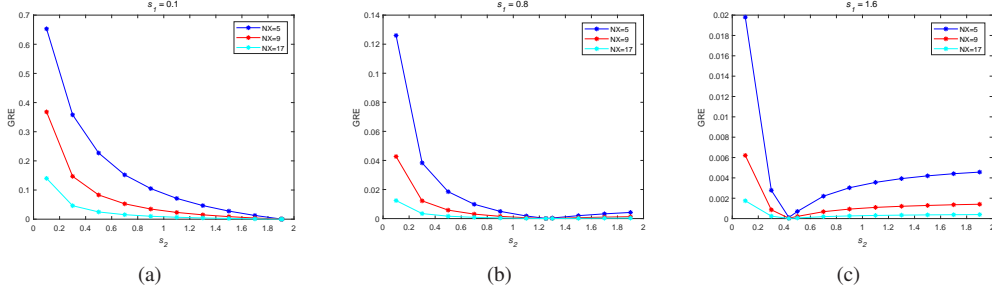


Figure 14: (Color online) The GREs of D2Q9 MRT model with ABB boundary scheme and weight coefficient $\omega_0 = 1/3$, $\omega_1 = 1/9$, $\omega_5 = 1/18$.

Table 8: The GREs of D2Q5 MRT model for the complex cases with ABB boundary scheme ($\omega_0 = 1/3$, $\omega_1 = 1/6$).

Different models		$N = 5$	$N = 9$	$N = 17$
<i>MRT</i>	$\tau_r = 1.0, \tau_i = 0.5$	1.2775×10^{-16}	2.0708×10^{-9}	1.1467×10^{-7}
	$\tau_r = 10.0, \tau_i = 9.5$	4.1977×10^{-16}	1.2100×10^{-14}	1.9386×10^{-10}
	$\tau_r = 0.501, \tau_i = 0.001$	4.4416×10^{-6}	1.5648×10^{-5}	5.8706×10^{-5}

5.2. Discrete effect of the ABB boundary condition

In the D1Q3 model, when $k = 1$, $k = N$, Eqs. (82b) and (82a) can be written as

$$f_{-1}^1 = (1 - s_1)f_{-1}^2 + s_1 f_{-1}^{2,eq} + B\delta_t R. \quad (86a)$$

$$f_1^N = (1 - s_1)f_1^{N-1} + s_1 f_1^{N-1,eq} + B\delta_t R. \quad (86b)$$

Substituting Eq. (79a) into Eq. (86a), substituting Eq. (79b) into Eq. (86b), we can obtain

$$f_{-1}^1 = (1 - s_1)(\phi_2 - f_0^{2,eq} + A\delta_t R - f_1^2) + s_1 f_{-1}^{2,eq} + B\delta_t R. \quad (87a)$$

$$f_1^N = (1 - s_1)(\phi_{N-1} - f_0^{N-1,eq} + A\delta_t R - f_{-1}^{N-1}) + s_1 f_1^{N-1,eq} + B\delta_t R. \quad (87b)$$

In addition, substituting Eqs. (77) and (82a) into Eqs. (87a) and (87b) gives rise to

$$s_1 f_{-1}^1 = \omega_1 \phi_2 + (s_1 - 1)\omega_1 \phi_1 + \frac{(s_1 A - B)(1 - s_1) + B}{2 - s_1} \delta_t R. \quad (88a)$$

$$s_1 f_1^N = \omega_1 \phi_{N-1} + (s_1 - 1)\omega_1 \phi_N + \frac{(s_1 A - B)(1 - s_1) + B}{2 - s_1} \delta_t R. \quad (88b)$$

Table 9: The E_{max} of D2Q5 MRT model for the complex cases with ABB boundary scheme ($\omega_0 = 1/3, \omega_1 = 1/6$).

Different models		$N = 5$	$N = 9$	$N = 17$
<i>MRT</i>	$\tau_r = 1.0, \tau_i = 0.5$	1.1102×10^{-16}	2.5946×10^{-9}	1.3973×10^{-7}
	$\tau_r = 10.0, \tau_i = 9.5$	7.2165×10^{-16}	1.7431×10^{-14}	2.3966×10^{-10}
	$\tau_r = 0.501, \tau_i = 0.001$	6.4009×10^{-6}	2.2385×10^{-5}	8.4811×10^{-5}

Table 10: The GREs of D2Q5 MRT model for the complex cases with BB boundary scheme ($\omega_0 = 1/3, \omega_1 = 1/6$).

Different models		$N = 5$	$N = 9$	$N = 17$
<i>MRT</i>	$\tau_r = 1.0, \tau_i = 0.5$	3.2814×10^{-16}	1.4988×10^{-11}	1.0332×10^{-7}
	$\tau_r = 10.0, \tau_i = 9.5$	1.6129×10^{-11}	5.6665×10^{-11}	1.0665×10^{-9}
	$\tau_r = 0.501, \tau_i = 0.001$	2.8179×10^{-6}	1.2367×10^{-5}	5.2043×10^{-5}

On the other hand, the ABB scheme can be given by

$$f_1^1 = -f_{-1}^{1,+} + 2\omega_1\phi_0. \quad (89a)$$

$$f_{-1}^N = -f_1^{N,+} + 2\omega_1\phi_L. \quad (89b)$$

Substituting Eq. (82b) into Eq. (89a), and substitute Eq. (82a) into Eq. (89b), one can obtain

$$f_1^1 = -[(1 - s_1)f_{-1}^1 + s_1f_{-1}^{1,eq} + B\delta_t R] + 2\omega_1\phi_0, \quad (90a)$$

$$f_{-1}^N = -[(1 - s_1)f_1^N + s_1f_1^{N,eq} + B\delta_t R] + 2\omega_1\phi_L. \quad (90b)$$

Substituting Eqs. (89a) and (89b) into Eqs. (90a) and (90b), we can obtain

$$\omega_1(-\phi_2 + 3\phi_1 - 2\phi_0) = \left[\frac{(s_1A - B)(1 - s_1) + B}{2 - s_1} - A - B \right] \delta_t R, \quad (91a)$$

$$\omega_1(-\phi_{N-1} + 3\phi_N - 2\phi_L) = \left[\frac{(s_1A - B)(1 - s_1) + B}{2 - s_1} - A - B \right] \delta_t R, \quad (91b)$$

which can also be written as

$$\omega_1(-\phi_2 + 3\phi_1 - 2\phi_0) = \frac{-2 + s_1 + s_2 - s_1s_2 + w_1(s_1 - 2)(s_2 - 2)}{s_2(s_1 - 2)} \delta_t R, \quad (92a)$$

Table 11: The E_{max} of D2Q5 MRT model for the complex cases with BB boundary scheme ($\omega_0 = 1/3, \omega_1 = 1/6$).

Different models		$N = 5$	$N = 9$	$N = 17$
<i>MRT</i>	$\tau_r = 1.0, \tau_i = 0.5$	4.4409×10^{-16}	2.3118×10^{-11}	1.4393×10^{-7}
	$\tau_r = 10.0, \tau_i = 9.5$	2.2474×10^{-11}	7.3081×10^{-11}	1.6065×10^{-9}
	$\tau_r = 0.501, \tau_i = 0.001$	4.4960×10^{-6}	1.8838×10^{-5}	7.7969×10^{-5}

$$\omega_1(-\phi_{N-1} + 3\phi_N - 2\phi_L) = \frac{-2 + s_1 + s_2 - s_1 s_2 + w_1(s_1 - 2)(s_2 - 2)}{s_2(s_1 - 2)} \delta_r R. \quad (92b)$$

From Eq. (36), we have

$$\phi_1 = -\frac{\Delta\phi}{N^2} + (2N + 1)\frac{\Delta\phi}{N^2} - (4N + 1)\frac{\Delta\phi}{N^2} + \frac{1}{2}(\phi_s^{N+0.5} - \phi_s^{0.5}) + \phi_0 + \phi_s^{0.5}, \quad (93a)$$

$$\phi_2 = -\frac{4\Delta\phi}{N^2} + (2N + 1)\frac{2\Delta\phi}{N^2} - (4N + 1)\frac{\Delta\phi}{N^2} + \frac{3}{2}(\phi_s^{N+0.5} - \phi_s^{0.5}) + \phi_0 + \phi_s^{0.5}, \quad (93b)$$

$$\phi_{N-1} = -\frac{\Delta\phi}{N^2}(N - 1)^2 + (2N + 1)\frac{\Delta\phi}{N^2}(N - 1) - (4N + 1)\frac{\Delta\phi}{N^2} + (N - \frac{3}{2})(\phi_s^{N+0.5} - \phi_s^{0.5}) + \phi_0 + \phi_s^{0.5}, \quad (93c)$$

$$\phi_N = -\Delta\phi + (2N + 1)\frac{\Delta\phi}{N} - (4N + 1)\frac{\Delta\phi}{N^2} + (N - \frac{1}{2})(\phi_s^{N+0.5} - \phi_s^{0.5}) + \phi_0 + \phi_s^{0.5}. \quad (93d)$$

Substituting Eqs. (93a) and (93b) into Eq. (92a), and Eqs. (93c) and (93d) into Eq. (92b), we can obtain Eqs. (39)

and (40).

6. References

References

- [1] Y.-H. Qian, D. d'Humières, P. Lallemand, Lattice BGK models for Navier-Stokes equation, *EPL (Europhysics Letters)* 17 (6) (1992) 479.
- [2] C. K. Aidun, J. R. Clausen, Lattice-Boltzmann method for complex flows, *Annual review of fluid mechanics* 42 (2010) 439–472.
- [3] Z. Guo, C. Shu, *Lattice Boltzmann method and its applications in engineering*, Vol. 3, World Scientific, 2013.
- [4] J. Zhang, Lattice Boltzmann method for microfluidics: models and applications, *Microfluidics and Nanofluidics* 10 (1) (2011) 1–28.
- [5] Y. Qian, Simulating thermohydrodynamics with lattice BGK models, *Journal of scientific computing* 8 (3) (1993) 231–242.
- [6] L.-S. Luo, S. S. Girimaji, Theory of the lattice Boltzmann method: Two-fluid model for binary mixtures, *Physical Review E* 67 (3) (2003) 036302.
- [7] H. Zheng, C. Shu, Y.-T. Chew, A lattice Boltzmann model for multiphase flows with large density ratio, *Journal of Computational Physics* 218 (1) (2006) 353–371.
- [8] Z. Guo, C. Zheng, B. Shi, T. Zhao, Thermal lattice Boltzmann equation for low Mach number flows: decoupling model, *Physical Review E* 75 (3) (2007) 036704.

- [9] L. Wang, Y. Zhao, X. Yang, B. Shi, Z. Chai, A lattice Boltzmann analysis of the conjugate natural convection in a square enclosure with a circular cylinder, *Applied Mathematical Modelling* 71 (2019) 31–44.
- [10] B. Chopard, J.-L. Falcone, J. Latt, The lattice Boltzmann advection-diffusion model revisited, *The European Physical Journal Special Topics* 171 (1) (2009) 245–249.
- [11] J. Perko, R. A. Patel, Single-relaxation-time lattice Boltzmann scheme for advection-diffusion problems with large diffusion-coefficient heterogeneities and high-advection transport, *Physical Review E* 89 (5) (2014) 053309.
- [12] B. Servan-Camas, F. T.-C. Tsai, Lattice Boltzmann method with two relaxation times for advection–diffusion equation: third order analysis and stability analysis, *Advances in Water Resources* 31 (8) (2008) 1113–1126.
- [13] R. Huang, H. Wu, A modified multiple-relaxation-time lattice Boltzmann model for convection–diffusion equation, *Journal of Computational Physics* 274 (2014) 50–63.
- [14] I. Ginzburg, Truncation errors, exact and heuristic stability analysis of two-relaxation-times lattice Boltzmann schemes for anisotropic advection-diffusion equation, *Communications in Computational Physics* 11 (5) (2012) 1439–1502.
- [15] Z. Chai, N. He, Z. Guo, B. Shi, Lattice Boltzmann model for high-order nonlinear partial differential equations, *Physical Review E* 97 (1) (2018) 013304.
- [16] C. Pan, L.-S. Luo, C. T. Miller, An evaluation of lattice Boltzmann schemes for porous medium flow simulation, *Computers & fluids* 35 (8-9) (2006) 898–909.
- [17] N. Jeong, D. H. Choi, C.-L. Lin, Estimation of thermal and mass diffusivity in a porous medium of complex structure using a lattice Boltzmann method, *International Journal of Heat and Mass Transfer* 51 (15-16) (2008) 3913–3923.
- [18] L. Wang, C. Huang, X. Yang, Z. Chai, B. Shi, Effects of temperature-dependent properties on natural convection of power-law nanofluids in rectangular cavities with sinusoidal temperature distribution, *International Journal of Heat and Mass Transfer* 128 (2019) 688–699.
- [19] Y. Xuan, K. Zhao, Q. Li, Investigation on mass diffusion process in porous media based on Lattice Boltzmann method, *Heat and mass transfer* 46 (10) (2010) 1039–1051.
- [20] M. Hussain, E. Tian, T.-F. Cao, W.-Q. Tao, Pore-scale modeling of effective diffusion coefficient of building materials, *International Journal of Heat and Mass Transfer* 90 (2015) 1266–1274.
- [21] Z. Chai, H. Liang, R. Du, B. Shi, A lattice Boltzmann model for two-phase flow in porous media, *SIAM Journal on Scientific Computing* 41 (4) (2019) B746–B772.
- [22] I. Ginzbourg, P. Adler, Boundary flow condition analysis for the three-dimensional lattice Boltzmann model, *Journal de Physique II* 4 (2) (1994) 191–214.
- [23] X. He, Q. Zou, L.-S. Luo, M. Dembo, Analytic solutions of simple flows and analysis of nonslip boundary conditions for the lattice Boltzmann BGK model, *Journal of Statistical Physics* 87 (1-2) (1997) 115–136.
- [24] Z. Guo, B. Shi, T. Zhao, C. Zheng, Discrete effects on boundary conditions for the lattice Boltzmann equation in simulating microscale gas flows, *Physical Review E* 76 (5) (2007) 056704.
- [25] Z. Guo, C. Zheng, Analysis of lattice Boltzmann equation for microscale gas flows: relaxation times, boundary conditions and the Knudsen layer, *International Journal of Computational Fluid Dynamics* 22 (7) (2008) 465–473.
- [26] Z. Chai, B. Shi, Z. Guo, J. Lu, Gas flow through square arrays of circular cylinders with Klinkenberg effect: a lattice Boltzmann study, *Communications in Computational Physics* 8 (5) (2010) 1052.
- [27] J. Lu, H. Han, B. Shi, Z. Guo, Immersed boundary lattice Boltzmann model based on multiple relaxation times, *Physical Review E* 85 (1) (2012) 016711.
- [28] J. Ren, P. Guo, Z. Guo, Rectangular lattice Boltzmann equation for gaseous microscale flow, *Advances in Applied Mathematics and Mechanics* 8 (2) (2014) 306–330.
- [29] T. Zhang, B. Shi, Z. Guo, Z. Chai, J. Lu, General bounce-back scheme for concentration boundary condition in the lattice-Boltzmann method,

- 220 Physical Review E 85 (1) (2012) 016701.
- [30] S. Cui, N. Hong, B. Shi, Z. Chai, Discrete effect on the halfway bounce-back boundary condition of multiple-relaxation-time lattice Boltzmann model for convection-diffusion equations, Physical Review E 93 (4) (2016) 043311.
- [31] I. Ginzburg, Prediction of the moments in advection-diffusion lattice Boltzmann method. II. Attenuation of the boundary layers via double- Λ bounce-back flux scheme, Physical Review E 95 (1) (2017) 013305.
- 225 [32] I. V. Karlin, F. Bösch, S. Chikatamarla, Gibbs' principle for the lattice-kinetic theory of fluid dynamics, Physical Review E 90 (3) (2014) 031302.
- [33] Z. Guo, C. Zheng, B. Shi, Lattice Boltzmann equation with multiple effective relaxation times for gaseous microscale flow, Physical Review E 77 (3) (2008) 036707.
- [34] Z. Chai, B. Shi, Z. Guo, A multiple-relaxation-time lattice Boltzmann model for general nonlinear anisotropic convection-diffusion equations, Journal of Scientific Computing 69 (1) (2016) 355-390.
- 230 [35] Y. Zhao, Y. Wu, Z. Chai, B. Shi, A block triple-relaxation-time lattice Boltzmann model for nonlinear anisotropic convection-diffusion equations, Computers and Mathematics with Applications.
- [36] A. J. Ladd, Numerical simulations of particulate suspensions via a discretized boltzmann equation. part 1. theoretical foundation, Journal of fluid mechanics 271 (1994) 285-309.
- 235 [37] Z. Guo, C. Zheng, B. Shi, Non-equilibrium extrapolation method for velocity and pressure boundary conditions in the lattice boltzmann method, Chinese Physics 11 (4) (2002) 366.
- [38] B. Shi, Z. Guo, Lattice Boltzmann model for nonlinear convection-diffusion equations, Physical Review E 79 (1) (2009) 016701.